foods

MDPI

Article

Ethanol Regulates Bitterness Perception of the Trp-Ile-Lys-Lys (WIKK) Peptide by Activating the Human Bitter Receptor T2R47

Xiangyun Cong [1,†], Ziyan Wu [1,2,†], Jihong Wu [1,*], Mingquan Huang [1], Weizheng Sun [3], Ying Sun [1], Dongrui Zhao [1] and Fuping Zheng [1]

[1] Key Laboratory of Brewing Molecular Engineering of China Light Industry, Beijing Technology and Business University, Beijing 100048, China
[2] College of Biosystems Engineering and Food Science, Zhejiang University, Hangzhou 310058, China
[3] School of Food Science and Engineering, South China University of Technology, Guangzhou 510640, China
* Correspondence: wujihong12@126.com
† These authors contributed equally to this work.

Abstract

This study investigated the modulatory mechanism of ethanol on bitter peptide perception using ethanol–water mixture models (38–62% ethanol) to elucidate the impact of bitter peptides on the sensory quality of Chinese Baijiu. Identified by the TastePeptidesDB and sensory evaluation, Trp-Ile-Lys-Lys (WIKK) exhibited markedly higher taste thresholds in ethanol–water than in water, and ethanol modulated WIKK's bitterness threshold through a non-monotonic pattern. Plasmid transfection and a Fluo-4 AM-based, flow-cytometric calcium mobilization assay in HEK293T cells confirmed that WIKK activated the human bitter receptor T2R47 with ethanol potentiating this activation. Molecular docking and dynamics simulations demonstrated WIKK bound human bitter receptor T2R47 primarily through H-bonds, π–π, and π–alkyl interactions in the ethanol–water system with the key binding sites of TRP88, HIS65, TYR85, ILE82, and ARG81, and ethanol significantly altered this binding affinity. These results elucidate ethanol's role in modulating peptide bitterness perception and the underlying molecular mechanisms, enhancing the understanding of Baijiu flavor complexity.

Keywords: bitterness peptides; human bitter receptor T2R47; ethanol; Baijiu; Trp-Ile-Lys-Lys

1. Introduction

Chinese Baijiu possesses multiple taste perceptions, such as sour, sweet, bitter, spicy, astringent, and salty that together form its defining unique flavor profile [1]. The primary stimuli associated with these tastes generally originate from nonvolatile compounds and their derivatives, such as organic acids, soluble sugars, alcohols, amino acids, and peptides. Recent studies have identified small peptides as key nonvolatile constituents in Baijiu. For instance, Wei et al. preliminarily identified 28 peptides composed of 3–9 amino acids in Fengxiang flavor-type Baijiu [2]. Huo et al. successfully identified 6 new peptides in Baijiu using high-performance liquid chromatography-quadrupole-time-of-flight-mass spectrometry (HPLC-QTOF-MS) from different flavor-types of Baijiu [3]. Despite these findings, most research on Baijiu peptides has focused on their bioactive properties, with limited attention given to their roles in shaping the taste and flavor of Baijiu [4–7]. Investigating peptide contributions to Baijiu's taste is critical for optimizing flavor quality, refining brewing processes, exploring health benefits, and advancing the mechanistic understanding

Check for updates

Academic Editor: Takafumi Mizushige

Received: 31 December 2025
Revised: 30 January 2026
Accepted: 14 February 2026
Published: 19 February 2026

Copyright: © 2026 by the authors. Licensee MDPI, Basel, Switzerland. This article is an open access article distributed under the terms and conditions of the Creative Commons Attribution (CC BY) license.

of its flavor chemistry, which underscores the scientific and practical significance of this research area.

Bitter substances have garnered attention in the food and beverage industry due to their unpleasant taste with higher concentrations and relatively low perception threshold [8]. As reported, polyphenols, iso-α-acids, higher alcohols, and peptides were commonly regarded as the main contributors to bitterness in alcoholic beverages [9]. This bitterness was mediated by 25 G protein-coupled receptors of the TAS2R family [10]. Pronin et al. [11] and Adler et al. [12] identified the T2R gene in humans and mice. In addition, research indicated that some receptors could be activated by multiple compounds, whereas others were specific to only a limited number of compounds [13]. The activation of distinct bitter receptors by specific bitter substances was usually determined through in vitro measurements and corresponding changes in Ca^{2+} currents [14]. The taste of peptides has been characterized using a combination of sensory and instrumental analysis [15]. Moreover, chemometric methods, including molecular docking and molecular dynamics simulations, offered new insights into the interactions between taste peptides and receptors [16] and could be integrated with sensory and instrumental analysis for a more comprehensive understanding [17]. However, the molecular basis of peptide-induced bitterness remained poorly understood. Ethanol, generally comprising 38% to 71% (v/v) of Baijiu, is central to shaping the taste and flavor of Baijiu [18]. Research has shown that ethanol enhanced Baijiu's bitterness perception at higher concentrations, likely through sensory interactions with other flavor components [19], and modulated the interfacial distribution of flavor compounds in ethanol–water mixtures [20]. These observations suggest that ethanol might influence bitter receptor activation, thereby affecting sensory bitterness perception. However, the precise nature of this effect and its underlying mechanisms require clarification.

Nevertheless, a systematic understanding of how bitter peptides are perceived in the high-ethanol environment characteristic of Baijiu remains limited. While the transduction mechanisms for specific bitter peptides have been established in aqueous systems through receptors such as T2R1 and T2R4 [21], and ethanol itself has been reported to activate receptors including T2R38 and influence overall bitterness perception [22], these two lines of investigation have remained largely separate. Consequently, the critical ternary interaction involving ethanol, bitter peptides, and taste receptors remains unelucidated. Specifically, it is still unclear how ethanol as a solvent and matrix component affects peptide-receptor recognition, binding, and downstream signaling. Key unresolved questions include whether and how ethanol alters peptide-receptor binding affinity, the conformational stability of the complex, and the efficiency of calcium-mediated signal transduction. This knowledge gap constrains a mechanistic understanding of the layered bitterness in spirits such as Baijiu and hinders flavor-driven product optimization.

To address this, the present study was designed to systematically investigate the modulatory effect of ethanol on the perception of a Baijiu-derived bitter peptide and its underlying molecular mechanism. Using the identified bitter peptide WIKK (Trp-Ile-Lys-Lys) and its potential target receptor T2R47 as the model system, we hypothesized that: (1) ethanol modulates the bitterness perception of WIKK by altering its binding mode to T2R47; and (2) ethanol enhances T2R47 activation by WIKK through the modulation of non-covalent interactions such as hydrogen bonds and π–π stacking. To test these hypotheses, the bitter taste threshold of WIKK was determined sensorially across a range of ethanol–water mixtures. Cellular calcium mobilization assays were then performed to evaluate WIKK-induced T2R47 activation in the presence of ethanol. Furthermore, molecular docking and molecular dynamics simulations were employed to elucidate, at the atomic level, the influence of ethanol on the peptide–receptor interaction pattern,

binding stability, and energetics. By integrating evidence from sensorial, cellular, and computational approaches, this work aims to clarify the molecular basis of the ethanol-mediated modulation of peptide bitterness and provides new mechanistic insights into the complex flavor composition of Baijiu.

2. Materials and Methods

2.1. Materials and Chemicals

Eighteen peptides (purity ≥ 98%), provided as trifluoroacetate (TFA) salts following HPLC purification, were synthesized by Shanghai Science Peptide Biological Technology Co., Ltd. (Shanghai, China). For cellular assays, stock solutions of the target peptide WIKK were prepared in sterile solvent and filter-sterilized (0.22 μm pore size) before use. Food grade anhydrous citric acid and monosodium glutamate were purchased from Lotus Co., Ltd. (Shanghai, China), while sucrose, quinine, and sodium chloride were obtained from Ganzhiyuan Co., Ltd. (Nanjing, Jiangsu, China). Reagents for cell culture and functional assays were of sterile, cell-culture grade. Fetal bovine serum, DMEM high-glucose medium, and Opti-MEM medium were purchased from Gibco (Thermo Fisher Scientific, Waltham, MA, USA). Lipofectamine 2000 transfection reagent was from Invitrogen (Thermo Fisher Scientific, Carlsbad, CA, USA). Phosphate-buffered saline (PBS), D-Hanks solution, and trypsin were sourced from Siwega Co., Ltd. (Wuhan, Hubei, China) and Biofroxx Co., Ltd. (Shanghai, China), respectively. The calcium-sensitive fluorescent dye Fluo-4 AM was supplied by Yeasen Co., Ltd. (Shanghai, China). The MonScript™ RT III All-in-One Mix with dsDNase and the SYBR® Green Pro Taq HS qPCR kit were purchased from Monad Co., Ltd. (Suzhou, Jiangsu, China) and Agbio Co., Ltd. (Changsha, Hunan, China), respectively. Absolute ethanol used for preparing ethanol-containing culture media was filter-sterilized (0.22 μm) before mixing with sterile medium. All cell manipulations were performed under aseptic conditions.

2.2. Prediction of Peptide Properties and Sensory Evaluation of Bitterness

2.2.1. Predicting the Bitter Taste, Solubility and Toxicity of the Peptides

The eighteen peptides from Baijiu listed in Table 1 were synthesized and collected based on previous literature reports. Their bitterness was initially predicted using the TastePeptidesDM (version 2024) of the TastePeptides-Meta platform (http://tastepeptides-meta.com/; accessed 26 June 2024), a comprehensive resource integrating database query, machine learning, and molecular docking for taste peptide evaluation [23]. For each peptide sequence, the module returns a binary classification ("Bitter" or "no-Bitter") along with a confidence score ("Pro Bitter"), representing the model's certainty in the prediction. The peptide property calculator (http://www.innovagen.com/; accessed 26 June 2024) was used to predict the solubility of the candidate peptides [24]. The water solubility was directly associated with biological availability. The toxicity prediction protocol in Discovery Studio 2019 software (Dassault Systèmes Biovia, San Diego, CA, USA) [25] and the ToxinPred web tool (https://webs.iiitd.edu.in/raghava/toxinpred/index.html; accessed 26 June 2024) [26] were used to evaluate the toxicity of the target peptides.

Table 1. Bitterness prediction results of the 18 reported Baijiu-derived peptides.

Amino Acid Composition	Abbreviation	Pro Bitter	Taste	Reference no.
Leu-Leu-Arg-Lys-Thr-Ser	LLRKTS	0.967	no-Bitter	[2]
Asp-Cys-Asn	DCN	0.944	no-Bitter	[3]
Pro-Pro-Asp-Gly	PPDG	0.941	no-Bitter	[27]
Ile-Phe-Glu-Val-Glu-Val-Asn-Lys	IFEVEVNK	0.939	no-Bitter	[2]
Asp-Arg-Ala-Arg	DRAR	0.873	no-Bitter	[27]
Leu-Leu-Leu-Ser-Leu-Lys-Lys	LLLSLKK	0.869	no-Bitter	[2]
Arg-Asn-His	RNH	0.844	no-Bitter	[28]
Leu-Leu-Lys-Val-Thr-Lys-Leu-Leu	LLKVTKLL	0.778	no-Bitter	[2]
Val-Cys-Trp-Asn	VCWN	0.349	Bitter	[3]
Ala-Lys-Arg-Ala	AKRA	0.107	Bitter	[5]
Leu-Leu-Leu-Leu-Leu-Leu-Leu-Leu	LLLLLLLL	0.068	Bitter	[2]
Leu-Trp-Leu-His-Gln-Lys	LWLHQK	0.068	Bitter	[2]
Ala-Cys-Phe	ACF	0.065	Bitter	[3]
Trp-ILe-Lys-Lys	WIKK	0.061	Bitter	[3]
Pro-His-Pro	PHP	0.06	Bitter	[6,29]
Lys-Val-Val-Ala	KVVA	0.046	Bitter	[3]
Cys-Trp-Cys	CWC	0.045	Bitter	[30]
Lys-Tyr	KY	0.042	Bitter	[3]

2.2.2. Sensory Evaluation of the Synthesized Peptides

Before the experiment started, the panelists were informed of the objectives, detailed experimental procedures, and sensory requirements for their participation. This study received approval from the ethics committee from Beijing Technology and Business University (BTBU) (No. 2024242). Twenty experienced sensory test panelists aged from 22 to 30 with good physical fitness, including 13 females and 7 males, were recruited from BTBU. The group members were trained prior to the evaluation as previously reported [31], fourteen panelists were selected for formal evaluation. Quantitative descriptive analysis (QDA) was performed to characterize the taste attributes of the peptides dissolved in purified water, with each panelist completing six replicate evaluations. Standard taste solutions were prepared according to GB/T 12315-2008 and GB/T 19547-2004 (China Standard Press) [32–34]. Panelists scored the intensity of five basic tastes including bitterness, umami, sourness, saltiness, and sweetness, using a discrete 10-point numerical scale (0 = not perceptible, 9 = extremely strong). It was verbally anchored at the endpoints (0 and 9) and chemically defined at points 1, 5, and 9 using reference solutions (Table S1), with intermediate integer scores employed for proportional rating between these anchors. The taste radar chart was constructed based on the mean intensity scores of the five attributes. Outliers were excluded using the triple standard deviation (3σ) method. Data processing details are provided in Section S1.1 in the Supplementary Materials.

2.3. Thresholds Evaluation of WIKK in Different Ethanol–Water Mixture Models

The taste thresholds of the target peptide, WIKK, was assessed via a modified triangle taste dilution assay (TDA) [35]. Ethanol–water mixtures spanning 38% to 62% (v/v) were prepared to model the typical ethanol content range of Chinese Baijiu. To overcome the masking effect of the dominant chemesthetic sensation of ethanol, WIKK stock solutions were prepared at a higher concentration of 8.0 mg·mL^{-1} in ethanol–water mixtures, compared to 1.0 mg·mL^{-1} in purified water, with complete dissolution confirmed. For each specified ethanol level (38%, 42%, 46%, 50%, 54%, 58%, and 62% v/v), a twofold serial dilution series of the peptide was prepared in the corresponding ethanol–water solvent. TDA was conducted by a trained panel of fourteen assessors. To mitigate the confounding effects of ethanol-induced trigeminal irritation, sensory fatigue, and cross-adaptation, the

evaluation of each ethanol concentration was carried out in an independent session on separate days. The presentation order of the seven ethanol levels was fully randomized across all assessors. Within a testing session, assessors were presented with a series of triads arranged in ascending order of WIKK concentration. Each triad comprised one sample containing WIKK and two blank controls (the corresponding ethanol–water mixture). Each assessor completed six replicates per ethanol condition, resulting in 84 triads per system (14 assessors × 6 replicates). Samples (10 mL) were served at (26 ± 0.5) °C in randomly coded, three-digit tasting cups. Assessors were instructed to expectorate the sample and then cleanse their palate with water, adhering to a mandatory 10-min rest interval between successive triads. Prior to the formal evaluations, all panelists underwent specific training to differentiate the bitter taste elicited by peptides from the trigeminal burning sensation caused by ethanol.

Data analysis was performed according to the method described by Wu et al. [36] with minor modifications. The base-10 logarithm of the WIKK concentration (ρ, mg·mL^{-1}) was plotted as the abscissa, and the corresponding correct recognition rate (Y) was plotted as the ordinate. The detection threshold was defined as the concentration at Y = 66.67%, a criterion based on chance correction for the triangle test (where chance = 33.33%). The 95% confidence intervals for these panel-level thresholds were calculated from the function fit.

$$X = \log_{10}\rho \quad (1)$$

$$Y = \frac{N_{correct}}{N_{total}} \quad (2)$$

where $N_{correct}$ represents the number of correct responses and N_{total} is the total number of triangle test trials.

2.4. Molecular Docking Analysis to Screen out the Potential Bitter Receptor

Three-dimensional models of 25 human bitter taste receptors were constructed using sequences from the UniProtKB database (https://www.uniprot.org/; accessed 16 July 2024) and the structure prediction platform AlphaFold (https://alphafold.ebi.ac.uk/; accessed 16 July 2024) [37]. The stereochemical quality of each homology model was evaluated using the PDBsum web server (http://www.ebi.ac.uk/pdbsum; accessed 16 July 2024) and the SAVES server (v6.0, https://saves.mbi.ucla.edu/; accessed 16 July 2024). Specifically, the Ramachandran plot generated by the PROCHECK tool within SAVES was used to assess the backbone conformation validity. This is a model that is considered suitable for molecular docking if >90% of its residues fall within the most favored regions. The total energy of each model was also evaluated via PDBsum. These validation steps collectively ensured the structural reliability of the models for subsequent molecular docking and dynamics simulations with small peptides [38]. Detailed procedures for the structural optimization of peptides and receptors, as well as docking validation, are described in Supplementary Materials, Sections S1.2 and S1.3 [39–41].

2.5. Exploration of T2R47 Activation in HEK293T Cells

2.5.1. Plasmid Transfection and qPCR Analysis

Primers for cloning the human bitter receptor T2R47 (GeneID: 259293) were designed using the NCBI protein database (https://www.ncbi.nlm.nih.gov/; accessed 20 August 2024) and incorporated flanking restriction sites for directional insertion into the pcDNA3.1(+) vector. The cloning primer sequences were: forward 5′-GGATCC ATGATAACTTTCTGCCCATCAT-3′ (BamHI site underlined) and reverse 5′-ACCGGTG CGAAGACACACAATGCCCCT-3′ (AgeI site underlined). Detailed protocols for cDNA synthesis and HEK293T cell culture are provided in Supplementary Materials,

Section S1.4 [13]. For transfection, a complex was prepared by combining 2.0 μg of the constructed plasmid (pcDNA3.1(+)-T2R47) in 250 μL Opti-MEM with 10 μL of Lipofectamine 2000 reagent (Invitrogen) in 250 μL Opti-MEM. After a 20-min incubation at room temperature, the mixture was added to cells in a 6-well plate. Transfected cells were maintained at 37 °C under 5% CO_2 for 48 h [42,43] and then observed using an inverted microscope (IX51, Olympus, Japan). Total RNA was extracted from adherent cells, and its concentration and purity were verified using a NanoDrop 2000 spectrophotometer (Thermo Fisher Scientific, Wilmington, DE, USA) and agarose gel electrophoresis. Reverse transcription was performed using the MonScript™ RT III All-in-One Mix with dsDNase (Monad). Quantitative PCR was carried out using the SYBR® Green Pro Taq HS premixed kit (Agbio) on a fluorescence quantitative PCR instrument. T2R47 transcript levels were quantified using the gene-specific primers: forward 5′-CAGTTTTGCGGCATGTGAGG-3′ and reverse 5′-GACACACAATGCCCCTCTTG-3′ (see Supplementary Table S2), which produce an 80-bp amplicon. GAPDH was used as the internal reference control. Relative gene expression was calculated using the ΔΔCT method [44–46].

2.5.2. Detection of Intracellular Calcium Mobilization by Flow Cytometry

To assess the effect of ethanol on WIKK-induced activation of the bitter receptor T2R47, culture media containing final ethanol concentrations of 38%, 42%, 46%, 50%, 54%, 58%, and 62% (v/v) were prepared as denoted Y_1 to Y_7 (see Table S3). For stimulation, 1.9 mL aliquots of each medium (Y_1–Y_7) were mixed with 100 μL of WIKK solution (20 mg·mL^{-1}) and vortexed; these were designated as X_1 to X_7. Thus, cells in groups X_1–X_7 were exposed to the corresponding high ethanol concentrations throughout the assay. In parallel, two control media were included: J_1 (physiological saline in complete medium) and J_2 (complete medium containing 54% (v/v) ethanol). T2R47-transfected HEK293T cells were incubated in media X_1–X_7, J_1, or J_2 for 30 min to capture the acute calcium response prior to potential cytotoxic effects. Prior to fluorescence analysis, a live-cell gate was defined based on forward scatter (FSC) and side scatter (SSC) parameters to exclude debris and non-viable cells, ensuring that the signals analyzed originated from a morphologically intact cell population. Intracellular calcium mobilization was then monitored using Fluo-4 AM labeling followed by flow cytometry, as previously described [47] and detailed in Supplementary Materials, Section S1.5.

2.6. Interaction Mechanism Between WIKK and T2R47

2.6.1. Theoretical Calculation of Active Sites Using Density Functional Theory

The molecular-level active sites of WIKK were investigated using density functional theory (DFT) method [48–50]. The three-dimensional structure of WIKK was first fully geometry-optimized in the gas phase at the B3LYP/6-311G(d,p) level of theory using Gaussian 09. Subsequently, single-point energy calculations were performed on the optimized geometry under two solvent environments (water and ethanol) using the same functional and basis set, with solvation effects incorporated via the Polarizable Continuum Model in the integral equation formalism (IEFPCM). Frontier molecular orbital analysis, focusing on the highest occupied molecular orbital (HOMO) and the lowest unoccupied molecular orbital (LUMO), was then carried out on the solvent-phase electronic structures using Multiwfn (version 3.8) and VMD [50] This analysis provided insights into the chemical reactivity and potential interaction sites of the peptide [51]. All structures were visualized with GaussView 5.0 (Gaussian Inc., Wallingford, CT, USA).

2.6.2. Molecular Dynamics Simulation

The current study explored the dynamic interactions between small peptides and bitter taste receptors, building upon prior findings that molecular docking reflects static interac-

tions. To further validate these findings, molecular dynamics simulation was performed according to the reference with minor revision [52]. The stability of the small peptides in binding to receptors was assessed in various ethanol–water mixtures (38%, 42%, 46%, 50%, 54%, 58%, and 62% v/v) using GROMACS 2019.6 software (Department of Biophysical Chemistry, University of Groningen, Groningen, The Netherlands). Utilizing PyMOL 3.0.4 software, the receptor and peptide complexes were separated and saved in .pdb and .mol2 formats. These .mol2 files were then processed using VMware to generate the necessary .itp and .gro format files for dynamic simulations. The specific procedure is described in Section S1.6 in the Supplementary Materials [53,54].

2.7. Thermodynamic Study

2.7.1. Binding Free Energy Calculations for WIKK and the Receptor

The molecular mechanics-Posson–Boltzmann surface area (MM-PBSA) method is a two-point free binding energy calculation technique that assesses the conformation of the system before and after binding without requiring sampling of the transition state [55]. These calculations were performed using the g_mmpbsa tool with an implicit solvent model, for which all parameters, including the dielectric constant, were set to the standard values for pure water (ε = 78.5) [56]. This provides a consistent framework for the comparative analysis of binding energies across the different ethanol–water systems studied. To elucidate the changes in binding free energy (ΔG_{bind}) of the protein–ligand complex, three energetic terms were included in the MM-PBSA analysis, including E_{MM}, ΔG_{sol}, and $-T\Delta S$. The relationship among them is shown in Equation (3) as follows. In this formula, ΔG_{bind} represents the binding free energy of the protein–ligand complex, E_{MM} represents the average molecular mechanical potential energy in a vacuum, ΔG_{sol} represents the free energy of solvation, and $-T\Delta S$ represents the entropic contribution to the free energy. However, the entropic contribution ($-T\Delta S$) was not considered in this study as binding of the small peptide WIKK would not induce large-scale conformational changes in the T2R47 receptor [55].

$$\Delta G_{bind} = E_{MM} + \Delta G_{sol} - T\Delta S \quad (3)$$

2.7.2. Molecular Mechanics Potential Energy

The vacuum potential energy (E_{MM}) consists of bonded (E_{bonded}) and nonbonded ($E_{nonbonded}$) interactions. Equation (4) can be used with the molecular mechanics (MM) force field parameters [57,58]. In this formula, E_{bonded} represents the bonded interaction, whereas $E_{nonbond}$ represents the nonbonded interaction. Nonbonded interactions primarily involve electrostatic and van der Waals forces. E_{elec} is the electrostatic interaction, and E_{vdw} is the van der Waals force.

$$E_{MM} = E_{bonded} + E_{nonbonded} = E_{bonded} + (E_{elec} + E_{vdw}) \quad (4)$$

2.7.3. Free Energy of Solvation

The free energy of solvation is the energy required to transfer a solute from a vacuum to a solvent. The free energy of solvation can be calculated using the density functional method and integral equation theory with statistical mechanics. In the MM-PBSA method, the free energy of solvation can be calculated using an implicit solvent model, which is expressed as Equation (5). In this formula, ΔG_{PB} represents the polar solvation energy calculated by the Poisson–Boltzmann equation, whereas ΔG_{nP} represents the nonpolar solvation energy determined via solvent-accessible surface area.

$$\Delta G_{sol} = \Delta G_{PB} + \Delta G_{nP} \quad (5)$$

2.8. Statistical Analysis

Data analysis of sensory evaluation and molecular dynamics simulation experiments were performed using the software Origin 2021 (Origin Lab Corporation, Northampton, MA, USA). Flow Cytometry Experiment analysis was performed using the software GraphPad Prism 10 (GraphPad Software, San Diego, CA, USA) and expressed as the mean ± standard deviation.

3. Results and Discussion

3.1. Computational Prediction and Sensory Validation of Bitter Peptide WIKK in Baijiu

TastePeptides-Meta was developed and expanded as a comprehensive taste peptide universe that integrates taste peptide query, prediction, and Python language-assisted modeling. TastePeptides-Meta comprises TastePeptidesDB, the most informative taste peptide database; Auto_Taste_ML, the first open-source machine learning package in the taste field; and Umami_YYDS, an umami/bitterness prediction model with an accuracy of 89.6% [23]. TastePeptidesDM (http://tastepeptides-meta.com/TPDM; accessed 26 June 2024) was used in this study, with the taste results of the 18 Baijiu tripeptides and tetrapeptides predicted and shown in Table 1. The model assigned a value approaching zero to substances classified as bitter and consequently identified 10 peptides as bitter taste candidates in its predictive analysis. The water solubility and toxicity of WIKK were predicted using Innovate and ToxinPred [25], suggesting good solubility with no predicted toxicity and no mutagenicity, thus ensuring the safety of subsequent sensory evaluations of WIKK.

Sensory evaluation was conducted by a trained panel to validate the model predictions regarding the bitterness of the synthesized peptides [31,59]. Notably, synthetic peptides often carry a background astringency, commonly attributed to their salt forms [60]. To ensure that bitterness evaluation was not confounded by this factor, panelists were specifically trained to distinguish between bitterness and astringency. Furthermore, as all peptides were synthesized and handled identically, any underlying astringency was uniformly present across samples and thus did not affect the relative ranking of bitterness intensity. The taste radar map (Figure 1A) revealed that WIKK, CWC, VCWN, DRAR, and PHP exhibited pronounced bitterness, while ACF was only faintly bitter, whereas ACF was only faintly bitter, and AKRA, DCN, RNH, PPDG, and KVVA showed negligible bitterness. Among these, WIKK exhibited the strongest bitter intensity, confirming its selection as the target bitter peptide based on both the prediction and sensory results. Furthermore, the sensory impact of WIKK was assessed by spiking it into the authentic Baijiu sample, as displayed in Figure 1B. The addition of WIKK produced a marked, concentration-dependent increase in perceived bitterness while simultaneously reducing sweetness and sourness. It also notably altered mouthfeel attributes such as softness, fullness, and harmony. These results provided direct evidence that WIKK functions as a bitter-modulating peptide within the complex matrix of Baijiu.

3.2. Bitterness Threshold of WIKK Under Different Ethanol–Water Solution Systems

The calculation curve for taste thresholds is shown in Figure 2. Calculations revealed that the threshold of WIKK in water and ethanol solutions (38%, 42%, 46%, 50%, 54%, 58%, and 62% (v/v)) was 0.04, 2.45, 0.63, 2.95, 0.77, 0.53, 0.19, and 0.79 mg·mL^{-1}, respectively (Figure 2A–H). Notably, the taste thresholds of WIKK underwent a dynamic variation following ethanol treatment, characterized by an initial increase, followed by a decrease and a final rebound. Given this non-monotonic change, there was no direct linear correlation between ethanol content and the taste threshold of WIKK. Consequently, the specific mechanism underlying ethanol's regulation of WIKK's bitter taste perception

required further investigation. It was important to note that the determined thresholds of WIKK were orders of magnitude higher than its actual concentration reported in Baijiu (24.25 ± 1.69 μg/L) [3]. This substantial discrepancy suggests that WIKK is unlikely to contribute to Baijiu bitterness through a simple additive effect. Instead, as demonstrated in our spiking experiment (Figure 1B), WIKK could modulate the sensory profile when introduced into the authentic Baijiu matrix. This indicates that its sensory impact might stem from synergistic interactions with other constituents in the complex Baijiu system, a hypothesis that merits direct validation in future studies with multicomponent mixtures.

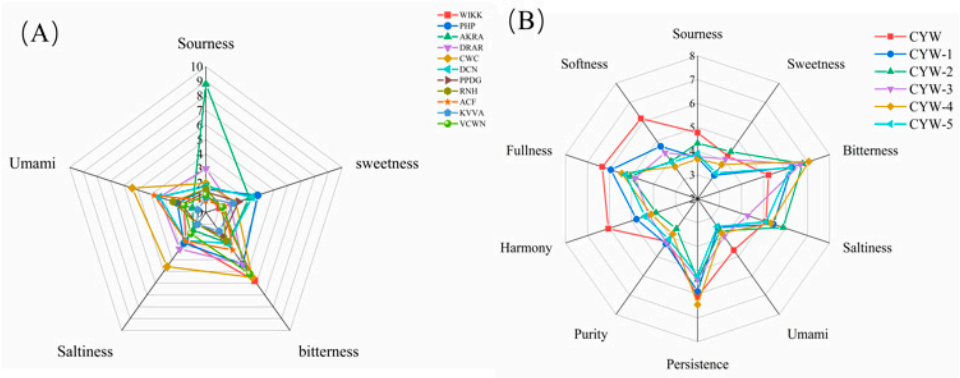


Figure 1. (**A**) Taste profiles of peptides obtained by quantitative descriptive analysis (QDA). Intensity was scored on a 0–9 scale with reference to defined chemical standards. (**B**) Changes in the sensory profile of Chinese Baijiu (CYW) upon the addition of WIKK at varying concentrations, evaluated for basic tastes and key mouthfeel attributes.

3.3. Expression of Bitter Taste Receptor T2R47 in HEK293T Cells

After transfection, HEK293T cells were observed by inverted microscopy (IX51, Olympus, Japan). Red fluorescence was detected under the excitation wavelength/bandwidth of 534/20 (524–544) and emission wavelength/bandwidth of 572/28 (558–586), suggesting successful transfection of the plasmid into HEK293T cells (Figure 3A). RNA quantitation by fluorescence quantitative PCR validated the specificity and purity of the products. Using the ΔΔCT method, T2R47 expression (2.17 ± 0.32) was found to be significantly upregulated by 2.17-fold compared to the control ($p < 0.05$), indicating successful transfection (Figure 3B) [46].

The activation of receptors could be observed through changes in cellular Ca^{2+} signal [61]. To verify the activation of the T2R47 bitter taste receptor by WIKK and the effect of ethanol, the Ca^{2+} signal of cells was detected by flow cytometry, and the expression level of markers was evaluated by measuring the average intensity of fluorescent dyes on cells. The higher the value, the stronger the expression of markers. Flow cytometry analysis was performed on a consistently gated population of single, intact cells, with the number of acquired events being high and comparable across all conditions (9142–9195 events per sample; see Supplementary Table S4), indicating stable data quality. As shown in Figure 3C, with the increase in ethanol content, the average fluorescence intensity showed an overall upward trend, which was more pronounced within the 50–62% range. This phenomenon might be attributed to the fact that ethanol can enhance the binding of WIKK to the bitter receptor T2R47. Furthermore, WIKK was more stable in 50–62% ethanol–water. This conclusion was consistent with previous research. To clarify the potential interference of ethanol on the fluorescence signal, this study specifically designed a saline–ethanol control experiment. As shown in Figure 3D, the fluorescence signal in cells treated with 54% (v/v) ethanol alone (J_2) exhibited only minimal fluctuations, comparable to those in the saline control (J_1). This result confirmed that ethanol itself, even at a concentration representing the upper half of the tested range, did not induce a nonspe-

cific calcium influx under the short-term exposure conditions used. By comparing these control data with the WIKK-mediated responses across ethanol concentrations (Figure 3C), two conclusions can be drawn: first, the solvent effect of ethanol on fluorescence detection was negligible under our experimental setup; second, the observed signal changes were attributable to the differential activation of T2R47 by WIKK in the presence of ethanol, rather than to any direct interference of ethanol with the detection system.

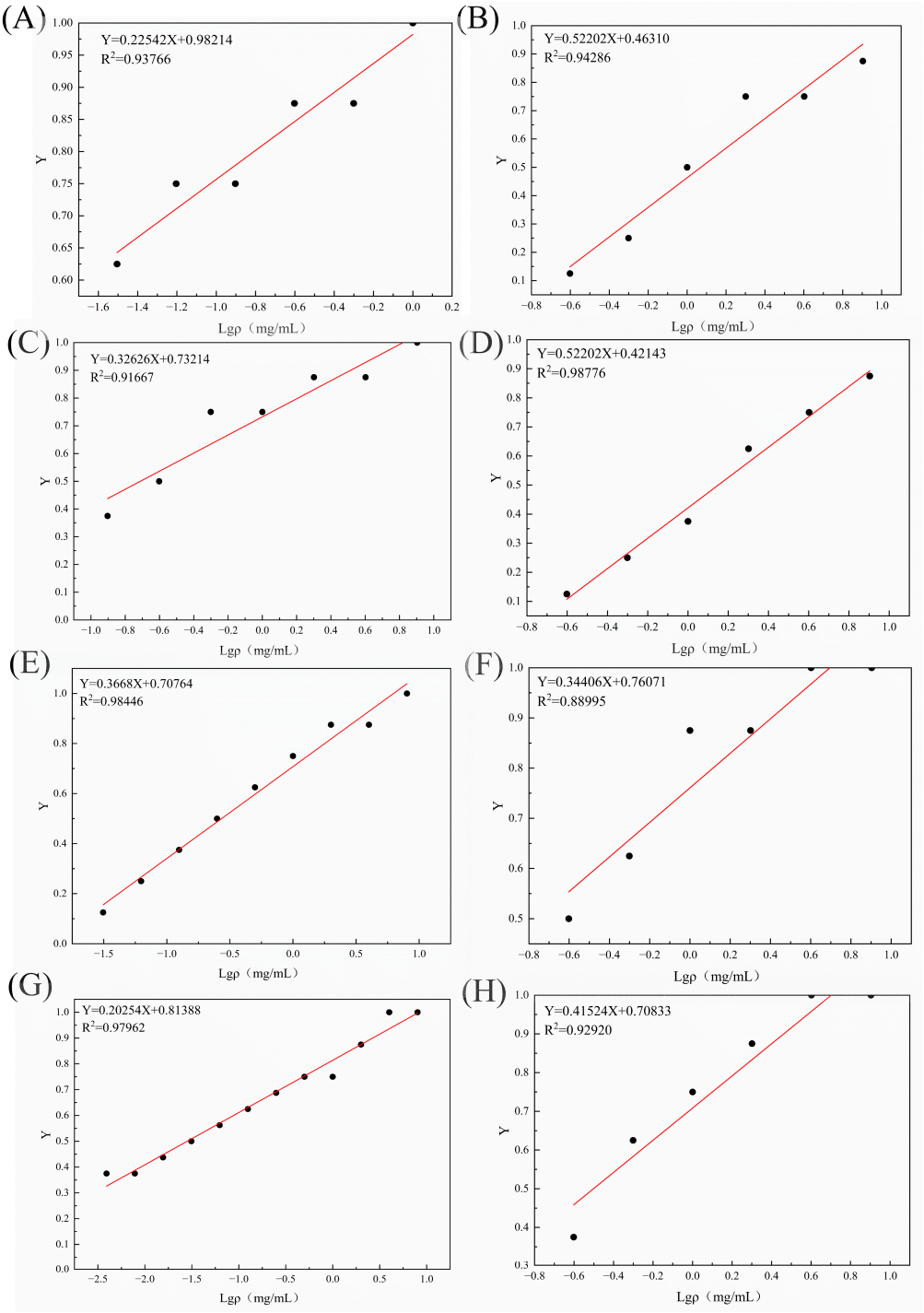


Figure 2. Fitting curves for WIKK thresholds in water and varying ethanol–water systems: (**A**) water, (**B**) 38%, (**C**) 42%, (**D**) 46%, (**E**) 50%, (**F**) 54%, (**G**) 58%, and (**H**) 62%.

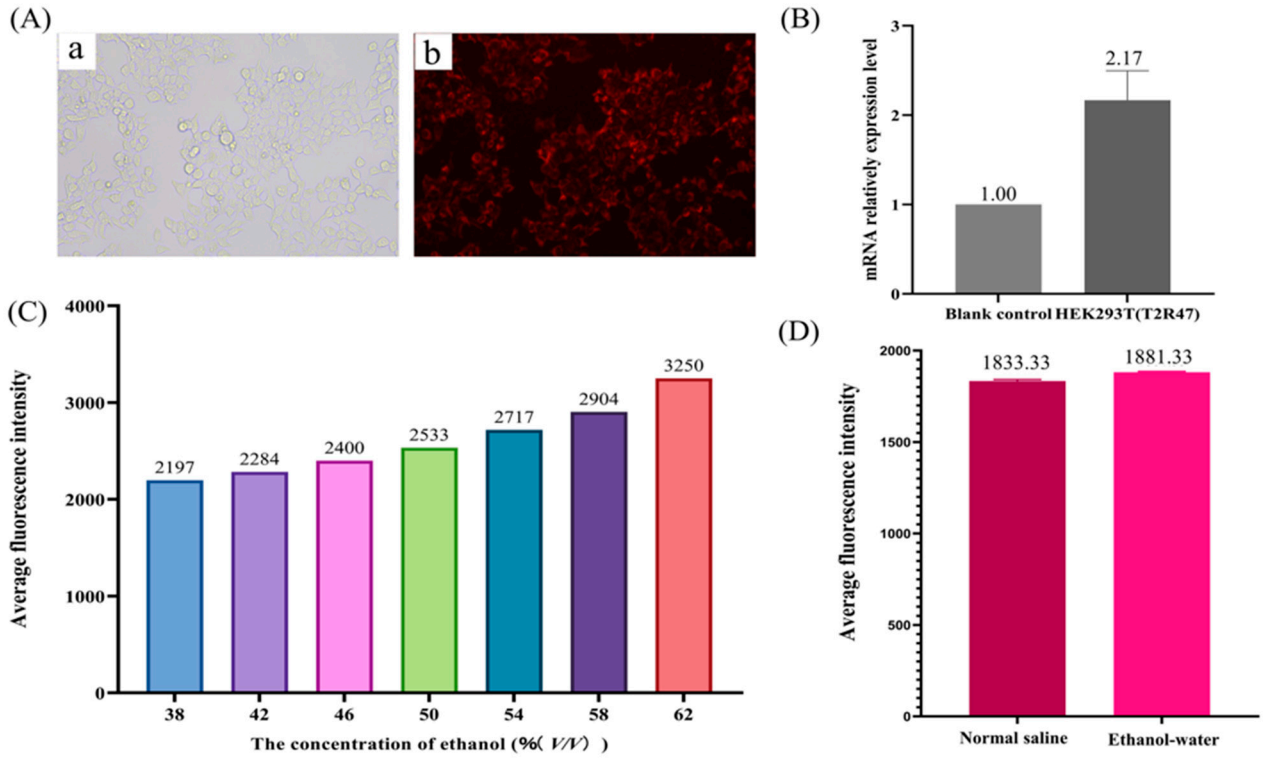


Figure 3. (**A**) T2R47 plasmid transfection validation (200X magnification): (**a**) bright-field and (**b**) fluorescence images of HEK293T cells; (**B**) Relative expression level of T2R47 mRNA in HEK293T cells; (**C**) Fluorescence intensity of WIKK-activated T2R47 receptor across an ethanol concentration gradient; (**D**) Average fluorescence intensity comparison between normal saline and ethanol–water systems.

3.4. Mechanism Analysis of WIKK Binding to Receptors

3.4.1. Theoretical Calculation of the Active Site of the Peptide

Density functional theory (DFT) calculations were performed to identify potential active sites of WIKK involved in receptor binding [46]. Analysis of the frontier molecular orbitals, specifically the highest occupied molecular orbital (HOMO) and the lowest unoccupied molecular orbital (LUMO), revealed regions prone to electron donation or acceptance, offering insights into sites likely to participate in noncovalent interactions such as π–π stacking or hydrophobic contact [62,63]. For WIKK, the DFT results localized the primary active site to the aromatic ring of the tryptophan residue, which exhibited high electron density in the HOMO (Figure 4A). This electronic characteristic remained stable in both aqueous and ethanolic environments, indicating its role as a persistent interaction hotspot. The prominence of tryptophan is consistent with its established contribution to peptide bitterness, as hydrophobic aromatic residues generally enhance bitter intensity and lower detection thresholds [21,64]. Importantly, the functional role of the tryptophan ring predicted by DFT was directly corroborated by subsequent molecular docking. The simulations demonstrated that the indole ring of tryptophan forms specific π–π and π–alkyl interactions with residues TYR85, ILE82, and ARG81 within the T2R47 binding pocket (Figure 4C,D and Table 2). The agreement between these independent computational approaches reinforces the conclusion that the tryptophan moiety is essential for WIKK binding and receptor activation. This integrated analysis yields a testable hypothesis: mutation of interfacial receptor residues such as TYR85, or chemical modification of the tryptophan side chain, should impair T2R47 activation and bitter taste perception, providing a clear direction for future experimental validation.

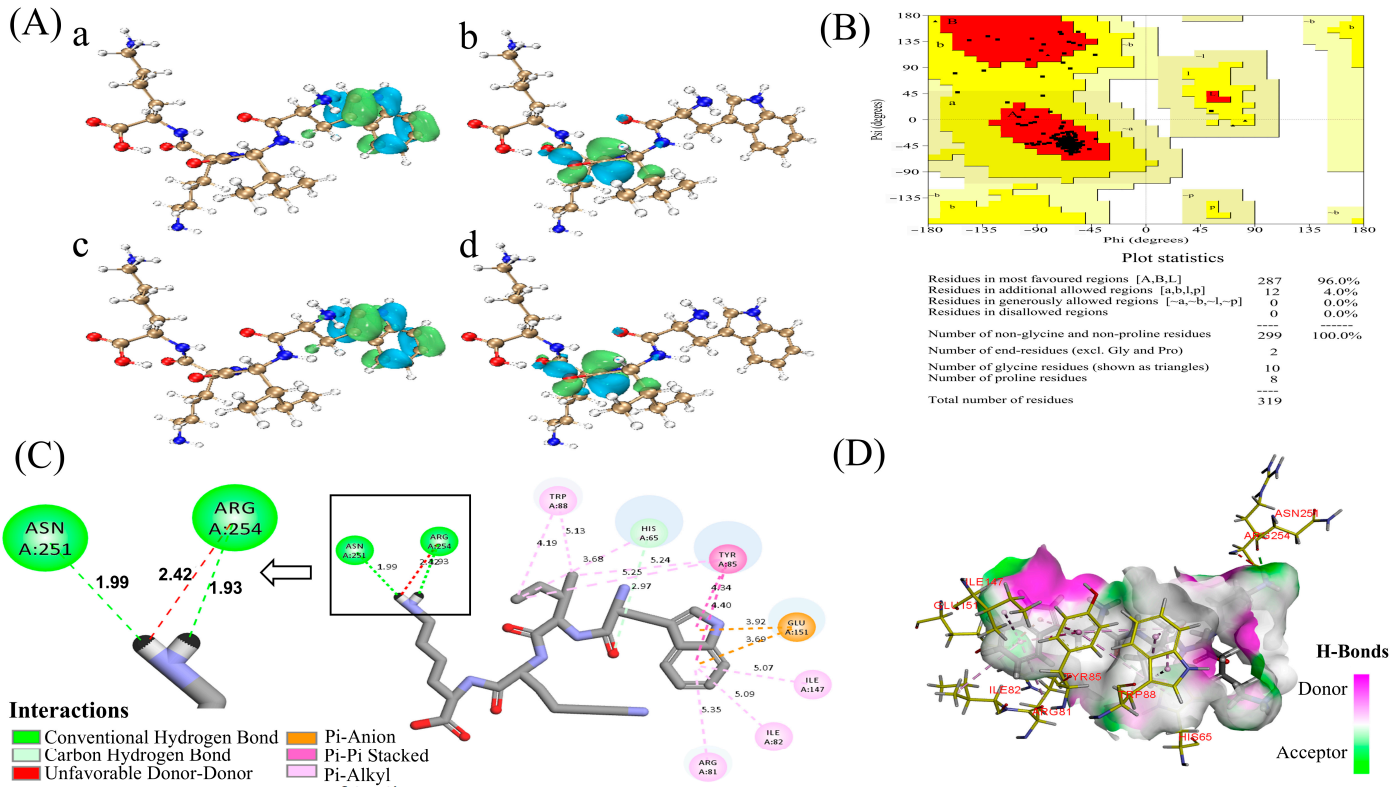


Figure 4. (**A**) Molecular orbital surfaces of WIKK (HOMO and LUMO) in (**a**,**b**) water and (**c**,**d**) ethanol. Oxygen atoms in red, nitrogen atoms in blue, carbon atoms in light brown, and hydrogen atoms (H) in white. The positive and negative phases of the wave function are shown in green and blue, respectively. (**B**) The Ramachandran plot of the homology model P59541 for bitter receptor T2R47; Red regions represent most favored regions, bright yellow regions indicate additionally allowed regions, light yellow correspond to generously allowed regions, white denote disallowed regions. (**C**) 2D and (**D**) 3D diagrams of the interaction force and binding sites between bitter receptor T2R47 and WIKK.

Table 2. Summary of 25 bitter taste receptors and their docking information with WIKK.

No.	Receptors	UniPort ID	Bitter DB ID	LibDock Score	Action Sites
1	T2R47	P59541	hTAS2R47	174.812	ASN251, ARG254, TRP88, HIS65, TYR85, GLU151, ILE147, ILE82, ARG81
2	TA2R8	Q9NYW2	hTAS2R8	173.904	PHE86, TRP89, SER251, TYR258, GLN82, GLU181, LEU183, ASP155, PRO182, LEU152
3	T2R19	P59542	hTAS2R48	172.546	GLU151, SER85, TYR76, ARG81, SER176, TRP154, GLN265, MET62, ILE245, ALA268, LEU65, TRP88
4	TA2R7	Q9NYW3	hTAS2R7	171.388	GLN6, LEU265, GLU264, LYS161, TYR76, PRO261, THR263, VAL160, ARG157
5	T2R20	P59543	hTAS2R49	170.207	HIS65, LEU64, PHE252, PHE249, TRP88, LEU245, ILE62, CYS244
6	TA2R1	Q9NYW7	hTAS2R1	167.712	ILE176, ILE174, SER178, GLN175, HIS144, LYS244, LYS251, LEU250, CYS82, CYS141
7	T2R31	P59538	hTAS2R44	166.761	TRP88, ASN65, LEU62, LYS265, PHE261, SER251, GLY253, SER248, PHE252, VAL249, LYS150, ALA177, THR180, ASP176
8	T2R42	Q7RTR8	hTAS2R42	166.49	LYS264, SER73, LYS267, THR77, ASP65, LEU156, TRP261, TYR76

Table 2. *Cont.*

No.	Receptors	UniPort ID	Bitter DB ID	LibDock Score	Action Sites
9	T2R16	Q9NYV7	hTAS2R16	166.428	GLN177, GLN151, ASN148, LEU74, CYS69, ASN66, LEU81, THR82, TYR76, LEU258, LYS254, PHE252, GLY249, ASP253, THR250, ARG255
10	T2R43	P59537	hTAS2R43	164.701	SER254, ASN257, SER251, PHE261, VAL249, THR180, PHE252, SER68, LYS265, TYR85
11	T2R39	P59534	hTAS2R39	154.745	PHE286, LYS114, TYR104, LEU101, ILE280, ASN293, TYR281, GLU93, TYR110, SER105
12	T2R10	Q9NYW0	hTAS2R10	153.643	GLU6, CYS249, VAL252, TRP162, LYS256, ILE69, GLN68, PHE250
13	TA2R3	Q9NYW6	hTAS2R3	153.538	HIS182, ASN257, TYR178, TYR155, GLU151, TYR189, ASP86, HIS76, ASP65, ALA253, LYS266, ALA265, THR90, PHE250
14	TA2R4	Q9NYW5	hTAS2R4	147.895	PHE69, THR66, ASN65, PHE84, PHE88, TYR250, ALA255, TYR254, LEU251
15	T2R45	P59539	hTAS2R45	147.499	THR82, TYR85, VAL147, LYS253, ARG81, TRP154, PHE252, SER251, LEU255, ASN254, LYS258
16	T2R13	Q9NYV9	hTAS2R13	144.094	GLU267, TYR263, GLU255, SER176, VAL179, PHE175, LEU82, LYS180, PHE172, ILE86
17	T2R14	Q9NYV8	hTAS2R14	137.570	LEU85, VAL180, SER265, SER254, GLU255, THR173, SER177, SER176, PHE172
18	TA2R9	Q9NYW1	hTAS2R9	136.409	ASN78, VAL82, SER83, SER79, HIS155, ASN149, LYS179, VAL171, SER172
19	T2R46	P59540	hTAS2R46	135.765	ASN76, ASN65, ALA84, GLU265, THR180, ILE181, ILE245, VAL249
20	T2R41	P59536	hTAS2R41	135.251	GLN83, TYR68, PHE84, GLY81, ARG82, GLU75, TYR76, LYS163, GLY78
21	TA2R5	Q9NYW4	hTAS2R5	132.29	GLN143, TRP165, ILE144, PHE148, PHE162
22	T2R60	P59551	hTAS2R60	131.501	LYS198, GLU190, ARG186, TYR89, PRO88, ASN163, PHE271, ALA97
23	T2R40	P59535	hTAS2R40	127.584	LEU82, ILE279, VAL18, LYS17, THR21, ASP7, ARG85, LYS11, LYS15, TYR274, SER14
24	T2R38	P59533	hTAS2R38	106.776	PHE252, LEU297, GLY300, LEU121, ALA245, LEU249, LYS120, LEU216
25	T2R50	P59544	hTAS2R50	88.6867	VAL260, PRO259, ASP258, LEU255, ASN257, ARG254, ARG253, ARG256, ILE2, TYR6

3.4.2. Molecular Docking Results

Molecular docking was performed to screen the interaction between WIKK and structural models of 25 human bitter taste receptors (hTAS2Rs). Based on the LibDock scores, the model P59541, corresponding to the bitter receptor hTAS2R47 (T2R47), showed the highest docking score with WIKK and was therefore selected for further investigation (Table 2). The stereochemical quality of the T2R47 homology model was evaluated using a Ramachandran plot. Analysis indicated that 96.0% of residues were located in the most favored regions, 4.0% in additionally allowed regions, and none in disallowed regions (Figure 4B), confirming the model's reliable backbone conformation and its suitability for subsequent computational analyses [65]. The docking interaction between WIKK and T2R47 yielded the lowest CDOCKER energy (−73.468 kcal/mol) among all receptors examined. Lower binding energy generally correlates with greater complex stability, which may facilitate bitterness perception [66]. This result supported the selection of T2R47 as the primary target receptor for experimental validation. Analysis of the binding mode revealed that WIKK interacts with T2R47 mainly through hydrogen bonding, π–π stacking, and π–alkyl

interactions. Key receptor residues involved in binding included ASN251, ARG254, TRP88, HIS65, TYR85, GLU151, ILE147, ILE82, and ARG81 (Figure 4C, D). Notably, the tryptophan residue of WIKK engaged in specific π–π and π–alkyl interactions with complementary residues TYR85, ILE82, and ARG81 in the T2R47 binding pocket, consistent with the role of aromatic hydrophobic residues in stabilizing bitter peptide–receptor complexes. These findings align with the DFT predictions, further indicating that the aromatic ring of tryptophan serves as a key active site for receptor binding.

3.4.3. Molecular Dynamics Simulation Analysis

The molecular docking results revealed that the small peptide WIKK could dock to the T2R47 receptor. To further understand the molecular conformation and stability of the small peptides WIKK and T2R47 in water and ethanol at 38%, 42%, 46%, 50%, 54%, 58%, and 62% (*v*/*v*), molecular dynamics simulation was performed. This model provides a theoretical reference for how different ethanol concentrations affect the bitterness perception of WIKK. Root Mean Square Deviation (RMSD) represents the distance between the same atoms in different structures. The RMSD of a protein can reveal the positional changes between its conformation and its initial conformation during the simulation process. The larger the RMSD value, the greater the deviation of the target molecule from the reference molecule [67]. For this study, RMSD could be used to characterize the stability of the protein structure and whether ligands have a depolymerization effect on the protein [68]. As shown in Figure 5A, the RMSD profiles revealed distinct stability patterns across ethanol concentrations. In the 38% and 46% ethanol systems, the WIKK ligand dissociated from the T2R47 binding pocket during the simulation (at approximately 12980 ps and 28570 ps, respectively), indicating poor complex stability under these conditions. In contrast, within the 50–62% ethanol range, the complex remained stably bound throughout the simulation, with lower and more consistent RMSD values. The computational stability trend aligned with the sensory threshold data. Specifically, the taste thresholds of WIKK were notably higher in the 38% and 46% ethanol systems, while they remained within a relatively stable and elevated range (0.53–0.79 mg·mL^{-1}) in the 50–62% ethanol range. The enhanced stability of the complex at higher ethanol concentrations suggests a molecular basis for the modulated bitterness response observed in sensory evaluations.

Radius of gyration (R_g) can characterize the compactness of protein structures and changes in the looseness of protein–peptide chains during simulation processes. Throughout the simulation, a lower and more consistent degree of fluctuation yielded higher stiffness and compactness of the system, resulting in a more stable protein structure [69]. Unique conformational changes or folding might lead to greater changes in R_g. RMSD and R_g values were frequently used for stability analysis [70]. As shown in Figure 5B, the Rg profile for the 38% ethanol system dropped markedly around 12.98 ns, coinciding with ligand dissociation, while a similar instability was observed at 28.57 ns in the 46% ethanol system. In contrast, within the 50–62% ethanol range, the Rg values remained lower and more stable, indicating increased structural compactness and complex stability with higher ethanol content, which aligns with the RMSD trends. The fluctuation of amino acid residues can be determined by root mean square fluctuation (RMSF), suggesting the average deviation of each amino acid from its reference position over time. Amino acids or amino acid groups with high RMSF values indicate greater flexibility, whereas low RMSF values suggest lower flexibility. Frequent fluctuations are regarded as indicative of poorer stability [71]. As illustrated in Figure 5C, the residue-level flexibility patterns were generally similar across all ethanol–water systems, suggesting that ethanol did not induce major localized conformational changes in the binding pocket.

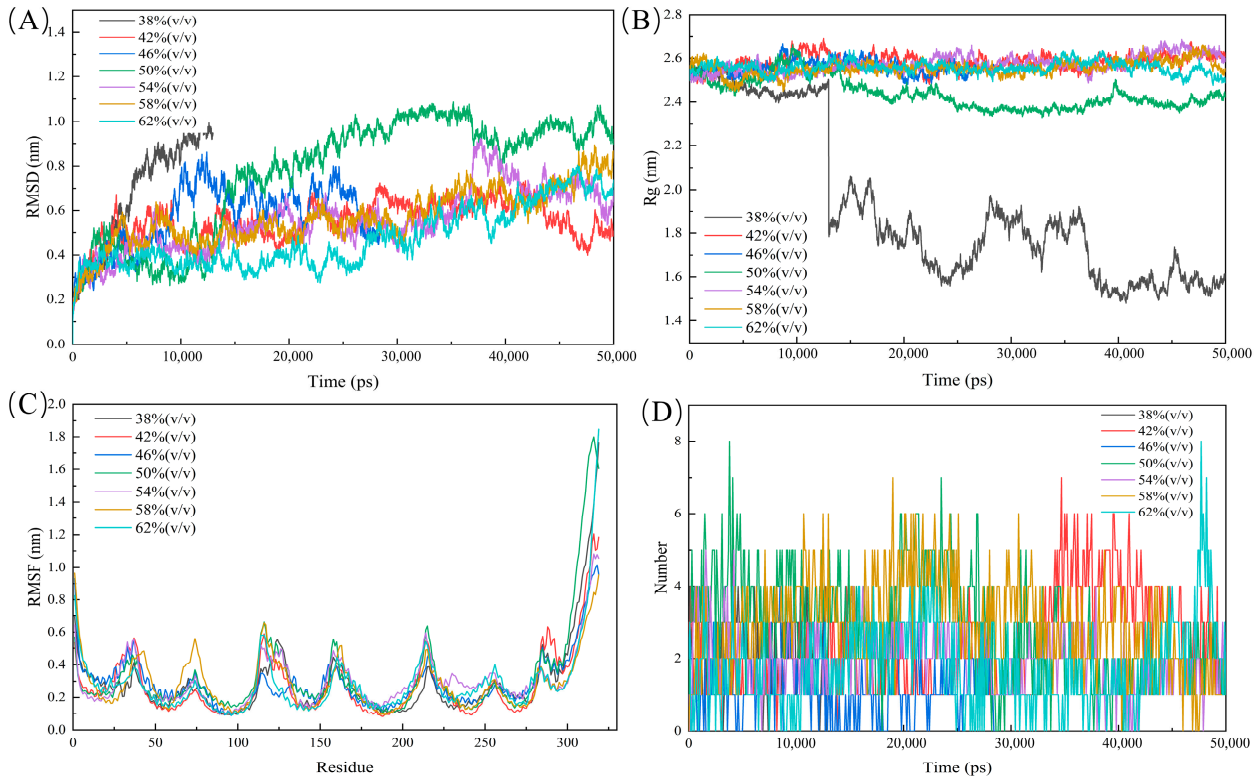


Figure 5. Molecular dynamics simulation analyses in ethanol–water systems: (**A**) root mean-square deviation (RMSD); (**B**) radius of gyration (Rg); (**C**) root mean-square fluctuation (RMSF); (**D**) hydrogen bond number.

The number of intermolecular hydrogen bonds between WIKK and T2R47 was quantified throughout the simulations using geometric criteria [52]. The average hydrogen-bond count varied non-monotonically across ethanol concentrations, following the order: 38% < 46% < 42% < 54% < 50% ≈ 62% < 58% (Figure 5D). This pattern mirrors the non-monotonic trends observed in both the MM-PBSA binding energies (Table 3) and the sensory taste thresholds (Figure 2), highlighting the complex, concentration-dependent role of ethanol in modulating the WIKK–T2R47 interaction landscape.

Table 3. Binding energy between WIKK and T2R47 under different systems.

Indicators	Binding Energy in Different Ethanol–Water Systems (KJ·mol^{-1})						
	38 (*v*/*v* %)	**42 (*v*/*v* %)**	**46 (*v*/*v* %)**	**50 (*v*/*v* %)**	**54 (*v*/*v* %)**	**58 (*v*/*v* %)**	**62 (*v*/*v* %)**
ΔG_{cou}	−100.792	−57.808	−89.187	−97.342	−57.792	−52.835	−69.906
ΔG_{vdw}	−334.496	−366.901	−271.899	−351.496	−339.432	−318.038	−318.627
ΔG_{PB}	260.896	267.057	256.406	272.815	215.408	227.829	241.698
ΔG_{nP}	−42.295	−43.564	−41.245	−42.486	−42.544	−43.452	−43.082
ΔG_{gas}	−435.289	−424.709	−361.087	−448.838	−397.224	−370.872	−388.533
ΔG_{sol}	218.601	223.493	215.161	230.329	172.864	184.377	198.616
ΔG_{bind}	−216.688	−201.216	−145.925	−218.50	−224.361	−186.496	−189.918

3.5. Thermodynamic Results and Analysis

The MM-PBSA binding energies (ΔG_{bind}) of the WIKK–T2R47 complex across the ethanol–water systems are summarized in Table 3. All values were negative, confirming that the interaction was thermodynamically favorable under all conditions examined [72]. Analysis of the ΔG_{bind} values revealed a non-monotonic trend with increasing ethanol content. While the binding energy was least favorable at 46% ethanol

(−145.925 kJ·mol^{-1}), it became substantially more favorable at 50% and 54% ethanol (−218.50 and −224.361 kJ·mol^{-1}, respectively). Notably, at even higher concentrations (58% and 62% ethanol), the binding energies weakened again (−186.496 and −189.918 kJ·mol^{-1}) but remained more favorable than at 46% ethanol. This complex, concentration-dependent profile aligns with the stability observed in molecular dynamics simulations (Figure 5A) and parallels the non-monotonic variations in the sensory taste thresholds across the same ethanol range (Figure 2). Together, these results suggest that ethanol modulates the WIKK–T2R47 interaction in a nuanced manner, potentially by influencing the balance of solvation, hydrophobic packing, and specific intermolecular forces. It should be noted that these calculations employed a pure-water implicit solvent model. Therefore, the absolute ΔG_{bind} values do not represent quantitatively precise binding free energies in each specific ethanol mixture, but they provide a consistent basis for comparing the relative changes in interaction strength across the conditions studied.

4. Conclusions

This study elucidated a dual role of ethanol in modulating the perception of the bitter peptide WIKK. Sensory analysis via modified TDA showed that ethanol significantly and non-monotonically elevated the bitterness threshold of WIKK. The TDA provided robust detection thresholds suitable for the complex ethanol–water matrix, though it could not quantify suprathreshold intensity or fully dissociate bitterness from the trigeminal effects of ethanol. In contrast, cellular assays demonstrated that ethanol enhanced WIKK-induced activation of the human bitter receptor T2R47. Computational simulations revealed that ethanol alters the binding mode between WIKK and T2R47, primarily through hydrogen bonding, π–π stacking, and π–alkyl interactions involving key residues (TRP88, HIS65, TYR85, ILE82, ARG81). Although the concentration of WIKK in Baijiu was below its isolated taste thresholds, our spiking experiment confirmed its capacity to modulate bitterness in the authentic Baijiu. This suggests that WIKK contributes to the overall bitterness profile not in an additive manner, but through synergistic interactions within the complex matrix of Baijiu, which is consistent with the receptor-level potentiation. Together, these results indicate that ethanol concurrently raises the detection threshold of peptides by affecting its interfacial accessibility and potentiates the signal output following receptor binding. The non-monotonic effects of ethanol highlight the complexity of taste perception in Baijiu. These findings provide molecular-level insights into ethanol-mediated taste modulation and advance the understanding of Baijiu flavor complexity. Future work should further validate receptor specificity, explore synergistic effects with other flavor compounds, and investigate the physiological relevance of peptide-mediated bitterness in complex food systems.

Supplementary Materials: The following supporting information can be downloaded at: https://www.mdpi.com/article/10.3390/foods15040751/s1, Section S1.1: Sensory evaluation of the synthesized peptides; Section S1.2: Optimization of the peptides and taste receptors structures; Section S1.3: The validity assessment of the docking between peptides and bitter taste receptors; Section S1.4: The cDNA sequence synthesis and HEK 293T cells culture protocols; Section S1.5: Intracellular calcium ion dynamics monitored using Fluo-4 AM labeling; Section S1.6: Molecular dynamics simulation conditions; Table S1: Taste evaluation criteria; Table S2: Primer sequences for target gene amplification; Table S3: Preparation of ethanol-containing culture media with graded concentrations; Table S4: Cell Event Counts and Mean Fluorescence Intensity.

Author Contributions: X.C.: Conceptualization and writing original draft. Z.W.: Writing and editing. J.W.: Conceptualization, writing, review, and editing. M.H.: Review. W.S.: Review. Y.S., D.Z. and F.Z.: Editing. All authors have read and agreed to the published version of the manuscript.

Funding: This work was supported by the National Natural Science Foundation of China (Grant numbers 32572739) and the National Key Research & Development Program of China (Grant numbers 2022YFD2101205).

Institutional Review Board Statement: This study was approved by the ethics committee from Beijing Technology and Business University (BTBU) (No. 2024242) on 20 November 2024.

Informed Consent Statement: Informed consent was obtained from all subjects involved in the study.

Data Availability Statement: All data generated or analyzed during this study are provided within the article and the Supplementary Materials. For any additional information, please contact the corresponding author.

Conflicts of Interest: The authors declare no conflicts of interest.

References

1. Dong, W.; Dai, X.; Jia, Y.; Ye, S.; Shen, C.; Liu, M.; Lin, F.; Sun, X.; Xiong, Y.; Deng, B. Association between Baijiu chemistry and taste change: Constituents, sensory properties, and analytical approaches. *Food Chem.* **2024**, *437*, 137826. [CrossRef] [PubMed]
2. Jia, W.; Du, A.; Dong, X.; Fan, Z.; Zhang, D.; Wang, R.; Shi, L. Physicochemical and molecular transformation of novel functional peptides from Baijiu. *Food Chem.* **2024**, *375*, 131894. [CrossRef]
3. Huo, J.; Ming, Y.; Li, H.; Li, A.; Zhao, J.; Huang, M.; Sun, W.; Wu, J.; Zhang, J. The protective effects of peptides from Chinese baijiu on AAPH-induced oxidative stress in HepG2 cells via Nrf2 signaling pathway. *Food Sci. Hum. Wellness* **2022**, *11*, 1527–1538. [CrossRef]
4. Li, Y.; Yuan, S.; Yong, X.; Zhao, T.; Liu, J. Research progress on small peptides in Chinese Baijiu. *J. Funct. Foods* **2020**, *72*, 104081. [CrossRef]
5. Wu, J.; Huo, J.; Huang, M.; Zhao, M.; Luo, X.; Sun, B. Structural characterization of a tetrapeptide from sesame flavor-type Baijiu and its preventive effects against AAPH-induced oxidative stress in HepG2 cells. *J. Agric. Food Chem.* **2017**, *65*, 10495–10504. [CrossRef]
6. Wu, J.; Sun, B.; Luo, X.; Zhao, M.; Zheng, F.; Sun, J.; Li, H.; Sun, X.; Huang, M. Cytoprotective effects of a tripeptide from Chinese Baijiu against AAPH-induced oxidative stress in HepG2 cells via Nrf2 signaling. *RSC Adv.* **2018**, *8*, 10898–10906. [CrossRef]
7. Li, H.; Fang, C.; Hu, Y.; Xu, J.; Zhao, W.; Li, L. The comparative analysis of peptides in enteral nutrition products and foods for special medical purposes. *Foods* **2024**, *13*, 2557. [CrossRef]
8. Li, H.; Li, L.; Zhang, Z.; Wu, C.; Yu, S. Sensory evaluation, chemical structures, and threshold concentrations of bitter-tasting compounds in common foodstuffs derived from plants and maillard reaction: A review. *Crit. Rev. Food Sci. Nutr.* **2023**, *63*, 2277–2317. [CrossRef]
9. Luo, Y.; Kong, L.; Xue, R.; Wang, W.; Xia, X. Bitterness in alcoholic beverages: The profiles of perception, constituents, and contributors. *Trends Food Sci. Technol.* **2020**, *96*, 222–232. [CrossRef]
10. Delompré, T.; Belloir, C.; Martin, C.; Salles, C.; Briand, L. Detection of bitterness in vitamins is mediated by the activation of bitter taste receptors. *Nutrients* **2022**, *14*, 4141. [CrossRef]
11. Pronin, A.; Xu, H.; Tang, H.; Zhang, L.; Li, Q.; Li, X. Specific alleles of bitter receptor genes influence human sensitivity to the bitterness of aloin and saccharin. *Curr. Biol.* **2007**, *17*, 1403–1408. [CrossRef]
12. Adler, E.; Hoon, M.; Mueller, K.; Chandrashekar, J.; Ryba, N.; Zuker, C. A novel family of mammalian taste receptors. *Cell* **2000**, *100*, 693–702. [CrossRef] [PubMed]
13. Xie, J.; Wen, H.; Shi, Y.; Wei, F.; Jiang, J.; Luo, L.; Zeng, L. Exploration of the mechanism of temperature influence on bitter taste of theacrine by activating human bitter taste receptor hTAS2R14. *Food Res. Int.* **2024**, *193*, 114857. [CrossRef]
14. Deng, S.; Zhang, G.; Aluko, O.; Mo, Z.; Mao, J.; Zhang, H.; Liu, X.; Ma, M.; Wang, Q.; Liu, H. Bitter and astringent substances in green tea: Composition, human perception mechanisms, evaluation methods and factors influencing their formation. *Food Res. Int.* **2022**, *157*, 111262. [CrossRef]
15. Hillmann, H.; Hofmann, T. Quantitation of key tastants and re-engineering the taste of Parmesan Cheese. *J. Agric. Food Chem.* **2016**, *64*, 1794–1805. [CrossRef] [PubMed]
16. Zhang, Y.; Gao, X.; Pan, D.; Zhang, Z.; Zhou, T.; Dang, Y. Isolation, characterization and molecular docking of novel umami and umami-enhancing peptides from Ruditapes philippinarum. *Food Chem.* **2021**, *343*, 128522. [CrossRef] [PubMed]
17. Liang, L.; Duan, W.; Zhang, J.; Huang, Y.; Zhang, Y.; Sun, B. Characterization and molecular docking study of taste peptides from chicken soup by sensory analysis combined with nano-LC-Q-TOF-MS/MS. *Food Chem.* **2022**, *383*, 132455. [CrossRef]
18. Liu, H.; Sun, B. Effect of fermentation processing on the flavor of Baijiu. *J. Agric. Food Chem.* **2018**, *66*, 5425–5432. [CrossRef]
19. Cretin, B.; Dubourdieu, D.; Marchal, A. Influence of ethanol content on sweetness and bitterness perception in dry wines. *LWT* **2018**, *87*, 61–66. [CrossRef]

20. Qin, D.; Shen, Y.; Yang, S.; Zhang, G.; Wang, D.; Li, H.; Sun, J. Whether the research on ethanol-water microstructure in traditional Baijiu should be strengthened? *Molecules* **2022**, *27*, 8290. [CrossRef]
21. Fu, Y.; Chen, J.; Bak, K.H.; Lametsch, R. Valorisation of Protein Hydrolysates from Animal By-Products: Perspectives on Bitter Taste and Debittering Methods: A Review. *Int. J. Food Sci. Technol.* **2019**, *54*, 978–986. [CrossRef]
22. Nolden, A.A.; McGeary, J.E.; Hayes, J.E. Differential Bitterness in Capsaicin, Piperine, and Ethanol Associates with Polymorphisms in Multiple Bitter Taste Receptor Genes. *Physiol. Behav.* **2016**, *156*, 117–127. [CrossRef] [PubMed]
23. Cui, Z.; Zhang, Z.; Zhou, T.; Zhou, X.; Zhang, Y.; Meng, H.; Wang, W.; Liu, Y. A TastePeptides-Meta system including an umami/bitter classification model Umami_YYDS, a TastePeptidesDB database and an open-source package Auto_Taste_ML. *Food Chem.* **2023**, *405*, 134812. [CrossRef] [PubMed]
24. Lafarga, T.; O'Connor, P.; Hayes, M. In silico methods to identify meat-derived prolyl endopeptidase inhibitors. *Food Chem.* **2015**, *175*, 337–343. [CrossRef]
25. Kan, R.; Yu, Z.; Zhao, W. Identification and molecular action mechanism of novel TAS2R14 blocking peptides from egg white proteins. *LWT* **2023**, *180*, 114716. [CrossRef]
26. Zhang, W.; Guan, H.; Wang, M.; Wang, W.; Pu, J.; Zou, H.; Li, D. Exploring the relationship between small peptides and the T1R1/T1R3 umami taste receptor for umami peptide prediction: A combined approach. *J. Agric. Food Chem.* **2024**, *72*, 13262–13272. [CrossRef]
27. Wu, J. Antioxidant Activity of Peptides from Sesame Flavor-Type Baijiu and Their Interactions with Aroma Compounds. Ph.D. Thesis, South China University of Technology, Guangzhou, China, 2018.
28. Huo, J.; Sun, B.; Zheng, F.; Sun, J.; Sun, X.; Li, H.; Luo, X.; Huang, M. Identification of a tripeptide Arg-Asn-His from Chinese Baijiu and its antioxidant activity. *Food Sci.* **2018**, *39*, 126–133.
29. Wu, J.; Sun, B.; Zhao, M.; Zheng, F.; Sun, J.; Sun, X.; Li, H.; Huang, M. Discovery of a bioactive peptide, an angiotensin converting enzyme inhibitor in Chinese Baijiu. *J. Chin. Inst. Food Sci. Technol.* **2016**, *16*, 14–20.
30. Huo, J.; Luo, X.; Huang, M.; Wu, J.; Zhang, J.; Liu, X.; Li, H.; Sun, X. Identification and antioxidant activity of a novel peptide from Baijiu. *Int. J. Pept. Res. Ther.* **2020**, *26*, 1199–1210. [CrossRef]
31. Li, M.; Liao, Q.; Wu, J.; Zhou, H.; Sun, Y.; Su, J.; Huang, M.; Zheng, J.; Zheng, F. Huangshui Polysaccharide: A Multifunctional Additive for Enhancing Antioxidant Activity, Aroma Profile, and Gut Health in Baijiu. *Int. J. Biol. Macromol.* **2025**, *333*, 148706. [CrossRef] [PubMed]
32. Shan, Y.; Pu, D.; Zhang, J.; Zhang, L.; Huang, Y.; Li, P.; Xiong, J.; Li, K.; Zhang, Y. Decoding of the Saltiness Enhancement Taste Peptides from the Yeast Extract and Molecular Docking to the Taste Receptor T1R1/T1R3. *J. Agric. Food Chem.* **2022**, *70*, 14898–14906. [CrossRef]
33. *GB/T 19547-2004/ISO 11056:1999*; Sensory analysis—Methodology—Magnitude estimation method. General Administration of Quality Supervision, Inspection and Quarantine & China National Standardization Administration: Beijing, China, 2004.
34. *GB/T 12315-2008/ISO 8587:2006*; Sensory analysis—Methodology—Ranking. General Administration of Quality Supervision, Inspection and Quarantine & China National Standardization Administration: Beijing, China, 2008.
35. Seo, W.; Lee, H.; Baek, H. Evaluation of bitterness in enzymatic hydrolysates of soy protein isolate by taste dilution analysis. *J. Food Sci.* **2007**, *73*, S41–S46. [CrossRef]
36. Wu, J.; Zheng, Y.; Sun, B.; Sun, X.; Sun, J.; Zheng, F.; Huang, M. The occurrence of propyl lactate in Chinese Baijius (Chinese Liquors) detected by direct injection coupled with Gas Chromatography-Mass Spectrometry. *Molecules* **2015**, *20*, 19002–19013. [CrossRef]
37. Huang, Y.; Shi, Y.; Liang, L.; Pu, D.; Zhang, X.; Zhang, Y. Research progress on perception and regulation of bitter compounds in foods. *Food Sci.* **2023**, *44*, 185–195.
38. Laskowski, R.; Jablonska, J.; Pravda, L.; Vareková, R.; Thornton, J. PDBsum: Structural summaries of PDB entries. *Protein Sci.* **2018**, *27*, 129–134. [CrossRef] [PubMed]
39. Yang, D.; Li, C.; Li, L.; Chen, S.; Hu, X.; Xiang, H. Taste mechanism of umami peptides from Chinese traditional fermented fish (Chouguiyu) based on molecular docking using umami receptor T1R1/T1R3. *Food Chem.* **2022**, *389*, 133019. [CrossRef]
40. Bai, G.; Pan, Y.; Zhang, Y.; Li, Y.; Wang, J.; Wang, Y.; Teng, W.; Jin, G.; Geng, F.; Cao, J. Research advances of molecular docking and molecular dynamic simulation in recognizing interaction between muscle proteins and exogenous additives. *Food Chem.* **2023**, *429*, 136836. [CrossRef] [PubMed]
41. Tokmakova, A.; Kim, D.; Guthrie, B.; Kim, S.-K.; Goddard, W.A.; Liggett, S.B. Predicted Structure and Cell Signaling of TAS2R14 Reveal Receptor Hyper-Flexibility for Detecting Diverse Bitter Tastes. *iScience* **2023**, *26*, 106422. [CrossRef]
42. Ke, J.; Cheng, J.; Luo, Q.; Wu, H.; Shen, G.; Zhang, Z. Identification of two bitter components in Zanthoxylum bungeanum Maxim. and exploration of their bitter taste mechanism through receptor hTAS2R14. *Food Chem.* **2021**, *338*, 127816. [CrossRef]
43. Chen, H.; Ren, X.; Wang, W.; Zhang, Y.; Chen, S.; Zhang, B.; Wang, L. Upregulated ROS production induced by the proteasome inhibitor MG-132 on XBP1 gene expression and cell apoptosis in Tca-8113 cells. *Biomed. Pharmacother.* **2014**, *68*, 709–713. [CrossRef]

44. Chen, Y.; Chen, H.; Hoffmann, A.; Cool, D.; Chappell, M.; Chen, A.; Morris, M. Adenovirus-mediated small-interference RNA for in vivo silencing of angiotensin AT_{1a} receptors in mouse brain. *Hypertension* **2005**, *47*, 230–237. [CrossRef]
45. Lei, Y.; Tang, L.; Xie, Y.; Y, X.; Zhang, L.; Wang, P.; Hamada, Y.; Jiang, K.; Zheng, W.; Jiang, X. Gold Nanoclusters-Assisted Delivery of NGF SiRNA for Effective Treatment of Pancreatic Cancer. *Nat. Commun.* **2017**, *8*, 15130. [CrossRef]
46. Upadhyaya, J.; Chakraborty, R.; Shaik, F.; Jaggupilli, A.; Bhullar, R.; Chelikani, P. The pharmacochaperone activity of quinine on bitter taste receptors. *PLoS ONE* **2016**, *11*, e0156347. [CrossRef]
47. Xu, Q.; Singh, N.; Hong, H.; Yan, X.; Yu, W.; Jiang, X.; Chelikani, P.; Wu, J. Hen protein-derived peptides as the blockers of human bitter taste receptors T2R4, T2R7 and T2R14. *Food Chem.* **2019**, *283*, 621–627. [CrossRef]
48. Huang, Z.; Zhang, W.; Zeng, Y.; Shi, S.; Wang, S.; Shen, C. Quantum chemistry calculation of hydrogen bond interactions between major compounds in Baijiu during storage. *Food Sci.* **2021**, *42*, 45–51.
49. Jia, W.; Du, A.; Fan, Z.; Wang, Y.; Shi, L. Effects of short-chain peptides on the flavor profile of Baijiu by the density functional theory: Peptidomics, sensomics, flavor reconstitution, and sensory evaluation. *J. Agric. Food Chem.* **2022**, *70*, 9547–9556. [CrossRef] [PubMed]
50. Chang, R.; Zhou, Z.; Dong, Y.; Xu, Y.; Ji, Z.; Liu, S.; Mao, J. Sensory-guided isolation, identification, and active site calculation of novel umami peptides from ethanol precipitation fractions of fermented grain Wine (Huangjiu). *Foods* **2023**, *12*, 3398. [CrossRef]
51. Lu, T.; Chen, F. Multiwfn: A multifunctional wavefunction analyzer. *J. Comput. Chem.* **2012**, *33*, 580–592. [CrossRef] [PubMed]
52. Zhao, W.; Zhang, Q.; Su, L.; Yu, Z. Taste characteristics and umami mechanism of novel umami peptides from hen egg proteins. *LWT* **2023**, *181*, 114778. [CrossRef]
53. Molitor, C.; Mauracher, S.G.; Rompel, A. Aurone synthase is a catechol oxidase with hydroxylase activity and provides insights into the mechanism of plant polyphenol oxidases. *Proc. Natl. Acad. Sci.* **2016**, *113*, 1806–1815. [CrossRef]
54. Maier, J.A.; Martinez, C.; Kasavajhala, K.; Wickstrom, L.; Hauser, K.E.; Simmerling, C. ff14SB: Improving the Accuracy of Protein Side Chain and Backbone Parameters from ff99SB. *J. Chem. Theory Comput.* **2015**, *11*, 3696–3713. [CrossRef]
55. Wang, J.; Wang, D.; Huang, M.; Sun, B.; Ren, F.; Wu, J.; Zhang, J.; Li, H.; Sun, X. Decoding molecular mechanism underlying human olfactory receptor OR8D1 activation by sotolone enantiomers. *J. Agric. Food Chem.* **2024**, *72*, 5403–5415. [CrossRef] [PubMed]
56. Kumari, R.; Kumar, R.; Lynn, A. g_mmpbsa-A GROMACS tool for high-throughput MM-PBSA calculations. *J. Agric. Food Chem.* **2014**, *54*, 1951–1962. [CrossRef] [PubMed]
57. Wang, J.; Wolf, R.; Caldwell, J.; Kollman, P.; Case, D. Development and testing of a general amber force field. *J. Comput. Chem.* **2004**, *25*, 1157–1174. [CrossRef]
58. Vidal-Limon, A.; Aguilar-Toalá, J.; Liceaga, A. Integration of molecular docking analysis and molecular dynamics simulations for studying food proteins and bioactive peptides. *J. Agric. Food Chem.* **2022**, *70*, 934–943. [CrossRef]
59. Dunkel, A.; Köster, J.; Hofmann, T. Molecular and sensory characterization of γ-glutamyl peptides as key contributors to the Kokumi taste of edible beans (*Phaseolus vulgaris* L.). *J. Agric. Food Chem.* **2007**, *55*, 6712–6719. [CrossRef]
60. Zhuang, M.; Lin, L.; Zhao, M.; Dong, Y.; Sun-Waterhouse, D.; Chen, H.; Qiu, C.; Su, G. Sequence, taste and umami-enhancing effect of the peptides separated from soy sauce. *Food Chem.* **2016**, *206*, 174–181. [CrossRef]
61. Lang, T.; Di-Pizio, A.; Risso, D.; Drayna, D.; Behrens, M. Activation profile of TAS2R2, the 26th human bitter taste receptor. *Mol. Nutr. Food Res.* **2023**, *67*, 2200775. [CrossRef]
62. Chakraborty, D.; Chattaraj, P. Conceptual density functional theory based electronic structure principles. *Chem. Sci.* **2021**, *12*, 6264–6279. [CrossRef] [PubMed]
63. Liao, L.; Qiu, C.; Liu, T.; Zhao, M.; Ren, J.; Zhao, H. Susceptibility of wheat gluten to enzymatic hydrolysis following deamidation with acetic acid and sensory characteristics of the resultant hydrolysates. *J. Cereal Sci.* **2010**, *52*, 395–403. [CrossRef]
64. Liu, B.; Li, N.; Chen, F.; Zhang, J.; Sun, X.; Xu, L.; Fang, F. Review on the release mechanism and debittering technology of bitter peptides from protein hydrolysates. *Compr. Rev. Food Sci. Food Saf.* **2022**, *21*, 5153–5170. [CrossRef]
65. Yu, Z.; Kang, L.; Zhao, W.; Wu, S.; Ding, L.; Zheng, F.; Liu, J.; Li, J. Identification of novel umami peptides from myosin via homology modeling and molecular docking. *Food Chem.* **2021**, *344*, 128728. [CrossRef]
66. Zhao, W.; Li, D.; Wang, Y.; Kan, R.; Ji, H.; Su, L.; Yu, Z.; Li, J. Identification and molecular docking of peptides from Mizuhopecten yessoensis myosin as human bitter taste receptor T2R14 blockers. *Food Funct.* **2021**, *12*, 11966–11973. [CrossRef]
67. Jia, R.; Yang, Y.; Liao, G.; Wu, H.; Yang, C.; Wang, G. Flavor characteristics of umami peptides from wuding chicken revealed by molecular dynamics simulation. *J. Agric. Food Chem.* **2024**, *72*, 3673–3682. [CrossRef]
68. Chen, X.; Duan, D.; Zhu, S.; Zhang, J. Molecular dynamics simulation of temperature induced unfolding of animal prion protein. *J. Mol. Model.* **2013**, *19*, 4433–4441. [CrossRef]
69. Yu, H.; Zhao, S.; Yi, J.; Du, M.; Liu, J.; Liu, Y.; Cai, S. Identification of novel umami peptides in termitornyces albuminosus (Berk) Heim Soup by In silico analyses combined with sensory evaluation: Discovering potential mechanism of umami taste formation with molecular perspective. *J. Agric. Food Chem.* **2023**, *71*, 17243–17252. [CrossRef] [PubMed]

70. Eslami-Farsani, R.; Shareghi, B.; Farhadian, S.; Momeni, L. Insight into the binding of glycerol with myoglobin: Spectroscopic and MD simulation approach. *Int. J. Biol. Macromol.* **2020**, *159*, 433–443. [CrossRef] [PubMed]
71. Honig, B.; Nicholls, A. Classical electrostatics in biology and chemistry. *Science* **1995**, *268*, 1144–1149. [CrossRef] [PubMed]
72. Ben, K.; Bouzid, M.; Mechi, N.; Ben-Lamine, A. Statistical physics modeling and interpretation of the adsorption of enantiomeric terpenes onto the human olfactory receptor OR1A1. *Int. J. Biol. Macromol.* **2021**, *171*, 428–434. [CrossRef]

Disclaimer/Publisher's Note: The statements, opinions and data contained in all publications are solely those of the individual author(s) and contributor(s) and not of MDPI and/or the editor(s). MDPI and/or the editor(s) disclaim responsibility for any injury to people or property resulting from any ideas, methods, instructions or products referred to in the content.